Purcell effect in hyperbolic metamaterial resonators

Alexey P. Slobozhanyuk,[1,2,*] Pavel Ginzburg,[3,4,†] David A. Powell,[1] Ivan Iorsh,[2] Alexander S. Shalin,[2,5,6] Paulina Segovia,[3] Alexey V. Krasavin,[3] Gregory A. Wurtz,[3] Viktor A. Podolskiy,[7] Pavel A. Belov,[2] and Anatoly V. Zayats[3]

[1]*Nonlinear Physics Center, Research School of Physics and Engineering, Australian National University, Canberra, ACT 0200, Australia*

[2]*Department of Nanophotonics and Metamaterials, ITMO University, St. Petersburg 197101, Russia*

[3]*Department of Physics, King's College London, Strand, London WC2R 2LS, United Kingdom*

[4]*Department of Physical Electronics, Fleischman Faculty of Engineering, Tel Aviv University, Tel Aviv 69978, Israel*

[5]*Kotel'nikov Institute of Radio Engineering and Electronics, RAS (Ulyanovsk branch), Ulyanovsk 432011, Russia*

[6]*Ulyanovsk State University, Ulyanovsk 432017, Russia*

[7]*Department of Physics and Applied Physics, University of Massachusetts Lowell, One University Avenue, Lowell, Massachusetts 01854, USA*

(Received 22 April 2015; revised manuscript received 12 August 2015; published 16 November 2015)

The radiation dynamics of optical emitters can be manipulated by properly designed material structures modifying local density of photonic states, a phenomenon often referred to as the Purcell effect. Plasmonic nanorod metamaterials with hyperbolic dispersion of electromagnetic modes are believed to deliver a significant Purcell enhancement with both broadband and nonresonant nature. Here, we have investigated finite-size resonators formed by nanorod metamaterials and shown that the main mechanism of the Purcell effect in such resonators originates from the supported hyperbolic modes, which stem from the interacting cylindrical surface plasmon modes of the finite number of nanorods forming the resonator. The Purcell factors delivered by these resonator modes reach several hundreds, which is up to 5 times larger than those in the ε-near-zero regime. It is shown that while the Purcell factor delivered by the Fabry-Pérot modes depends on the resonator size, the decay rate in the ε-near-zero regime is almost insensitive to geometry. The presented analysis shows a possibility to engineer emission properties in structured metamaterials, taking into account their internal composition.

DOI: 10.1103/PhysRevB.92.195127 PACS number(s): 81.05.Xj, 73.20.Mf, 78.67.Pt

I. INTRODUCTION

The local density of optical states (LDOS) related to various photonic modes can strongly affect quantum dynamics of light-matter interactions [1]. Free-space electromagnetic modes can be modified in the vicinity of material structures, and as a result, either a local enhancement or reduction of the interaction strength can be achieved. The rate of spontaneous emission in a weak light-matter coupling regime, calculated on the basis of the Fermi golden rule, is proportional to the LDOS, and its change relative to free space is referred to as a Purcell factor [2]. Furthermore, the formalism of the Purcell effect can be generalized to higher-order effects, such as spontaneous two-photon emission [3,4]. The Purcell enhancement in dielectric cavities is typically related to the ratio of the quality factor of the resonance to the volume occupied by the resonant mode. Various types of photonic cavities can deliver quality Q factors as high as 10^{10} and satisfy the conditions to reach the strong-coupling regime [5] where the Purcell factor description of decay dynamics breaks down [6]. Noble metal (plasmonic) nanostructures provide relatively low quality factors but yield subwavelength optical confinement [7] and, as a result, also efficiently influence spontaneous emission [8,9]. This nanoplasmonic approach is extremely beneficial for certain quantum optical applications, where improved and designed scattering cross sections are required to develop functionalities at the nanoscale and single-photon levels [10]. The Purcell enhancement in plasmonic nanostructures depends significantly on the relative position of the emitters with respect to a metal nanostructure, posing serious challenges and limitations for large-scale practical implementations [11]. Furthermore, the enhancement, based on local plasmonic resonances approach, still has a limited bandwidth, even though it is much broader than for high-Q optical cavities.

A qualitatively different approach to decay rate engineering relies on designing the hyperbolic dispersion of modes supported by anisotropic metamaterials, which ensures high nonresonant Purcell factors in a broad wavelength range [12]. These metamaterials with extreme anisotropy of dielectric permittivity, also known as hyperbolic metamaterials, have recently attracted significant attention due to their unusual electromagnetic properties. Homogenized hyperbolic metamaterials were theoretically shown to provide infinitely large LDOS and, as a result, are expected to deliver extremely high Purcell enhancements [13]. This diverging LDOS originates from the hyperbolic dispersion of modes in uniaxial crystals, having opposite sign of the permittivity components in the ordinary and extraordinary directions, perpendicular and parallel to the optical axis, respectively. The fundamental limitations for this type of enhancement result from a particular metamaterial realization as composites of finite-size components, commonly referred to as "meta-atoms" [14], as well as the metamaterials' nonlocal response [15,16]. The most widely used realizations of hyperbolic metamaterials are based on layered metal-dielectric structures [17] or vertically aligned nanorod arrays [18]. Hyperbolic metamaterials also serve as building blocks for optical components with enhanced capabilities, such as hyperbolic cavities [19] and waveguides [20], as well as delivering nonreciprocal effects [21], Hamiltonian optics-based cavities [22], and many others.

*Corresponding author: a.slobozhanyuk@phoi.ifmo.ru

†Corresponding author: pginzburg@post.tau.ac.il

In this work, we analyze emission properties of a radiating dipole embedded inside or in close proximity to a finite-size three-dimensional resonator formed by a nanorod-based hyperbolic metamaterial. Taking into account the details of the hyperbolic metamaterial realization as a finite number of plasmonic nanorods, we show that the Purcell enhancement originates from Fabry-Pérot modes of the resonator formed by the hyperbolic metamaterial. The impact of the modes of the metamaterial resonators on the Purcell factor has been investigated for different resonator sizes, and the importance of the emitter's position within the resonator has been considered. We also demonstrate the fast convergence of the Purcell enhancement with the increase of the number of nanorods in the resonator, with a 16×16 nanorod array having properties of an infinite metamaterial slab (infinite number of finite-length rods). This investigation enables comparison of the Purcell enhancement provided by both finite-size and infinite structures and separating the impact of the modal structure of resonators.

II. EFFECTIVE MEDIUM THEORY AND NUMERICAL MODELING

We consider a metamaterial consisting of a square array of plasmonic (Au) nanorods (Fig. 1). This basic configuration enables addressing all the relevant effects, with substrate and embedding dielectric materials straightforwardly included in numerical modeling. In the first approximation, neglecting nonlocal effects [23], the optical response of such a structure can be obtained from a homogenization procedure of the nanorod composite [24], representing it as an effective uniaxial medium with permittivity tensor $\varepsilon = \mathrm{diag}(\varepsilon_{xx},\varepsilon_{xx},\varepsilon_{zz})$, where $\varepsilon_{xx} = \varepsilon_{yy}$ and ε_{zz} are the permittivities for the light polarization

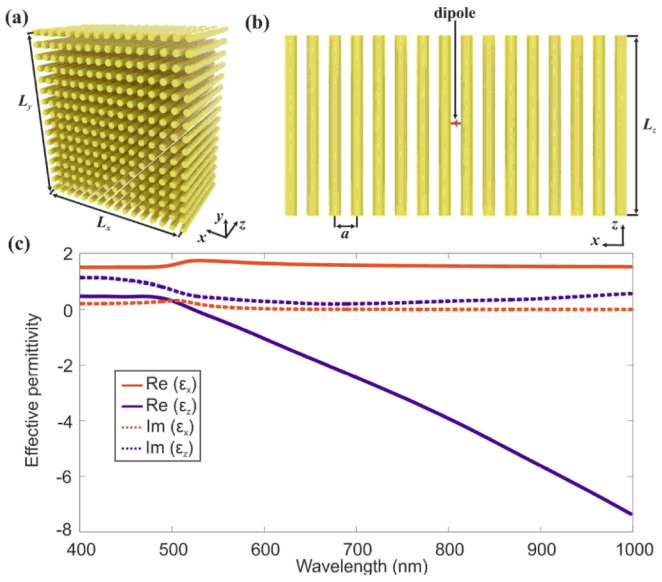

FIG. 1. (Color online) (a) Schematic view of the hyperbolic metamaterial resonator with the transverse dimensions L_x and L_y. (b) Schematics of the numerical setup. An emitting dipole is inserted in the center of the resonator. (c) The effective permittivity of the metamaterial calculated for an infinite array of nanorods with $L_z = 350\,\mathrm{nm}$, $a = 60\,\mathrm{nm}$, $r = 15\,\mathrm{nm}$ (Au permittivity was taken from [32]).

perpendicular to and along the nanorod axes, respectively [Figs. 1(a) and 1(b)]. In the frequency range where ε_{xx} and ε_{zz} have opposite signs [Fig. 1(c)], extraordinary electromagnetic modes, propagating in such an anisotropic medium, have hyperbolic dispersion. For the considered system, this crossing from the conventional elliptic to hyperbolic dispersion regime occurs at around 520-nm wavelength, where the real part of the effective permittivity ε_{zz} becomes vanishingly small [Fig. 1(c)]. The frequency range around $\mathrm{Re}(\varepsilon_{zz}) = 0$ is called the ε-near-zero (ENZ) region. This ability to support the quasistatic behavior of electromagnetic waves (freeze phase) has various intriguing consequences on wave propagation in bended structures [25] and in tailoring radiation properties [26]. It should be noted that the ENZ regime is usually linked with the strong spatial dispersion effects since the vanishing leading term in the permittivity coefficient makes the next term of significant importance [27].

The nonlocal (spatial dispersion) behavior of the nanorod metamaterials cannot be described in the conventional effective medium theory and has an impact on both reflection and transmission of the metamaterial as well as emission and nonlinear effects [23]. Electromagnetic nonlocalities could be classified as structural, material, and collective [28]. While constitutive material components of the considered metamaterial may, in principle, exhibit collective hydrodynamic-type nonlocalities [29], their contribution is small for the geometrical sizes considered here. Structural nonlocality due to the retardation effects in the unit cell is much stronger in the case of nanorod metamaterial, requiring modifications in the homogenization approach and the use of modified effective medium models [23,30]. Numerical modeling which considers the internal, microscopic structure of metamaterial composites takes the structural nonlocality into consideration automatically without a need for any additional considerations.

The numerical simulations have been performed using the time-domain solver of the CST MICROWAVE STUDIO 2014 package [31]. We used perfect matched layer (PML) boundaries, and additional space was added between the structure and the PMLs in order to prevent evanescent waves from interacting with the boundaries. Optical constants for gold were taken from Ref. [32]. The subwavelength dipolar emitter was modeled here as a perfect electric conductor (PEC) nanorod with a length of 28 nm and a radius of 1 nm [Fig. 1(b)]. The Purcell factor was calculated through an input impedance of a point dipole source. As was previously shown [33,34], this method is completely equivalent to the Green's function approach, which is widely used in photonics [35].The overall number of mesh cells was around 3×10^6, with mesh density locally adjusted in order to accurately represent the source. In order to reach reliable results and to prevent the oscillation of the output time signal after the excitation has been turned off, the duration of the simulation is usually increased above the interval needed to transmit the excitation pulse.

The numerical analysis based on the Green's function approach enables evaluation of both the decay rates, which are proportional to the imaginary part of the Green's function, and the energy shift, which is proportional to its real part [36]. A similar approach taking into account nonlocal response, Lamb shift, and linewidth modifications has recently been used for layered hyperbolic metamaterials [37]. The analysis,

reported here, concentrates on Purcell factor evaluation. Since the rate enhancement has not shown extremely high values, wavelength shift was neglected.

III. RESULTS

A. Hyperbolic metamaterial resonators

We begin with an analytical description of the modal structure of finite-size resonators made of a homogenized hyperbolic metamaterial based on the nanorod assembly. The Purcell factor is proportional to the imaginary part of the Green's function in a medium [1]:

$$R(\omega) = \mathrm{Im}G(\mathbf{r},\mathbf{r},\omega) \approx \mathrm{Im}\sum_{n,l,m,\sigma}\frac{\left|E_x^{n,l,m,\sigma}(\mathbf{r})\right|^2}{\omega^2-\omega_{n,l,m,\sigma}^2}, \quad (1)$$

where n, l, m are integers denoting the eigenmode number of the resonator made of the metamaterial and $\sigma = \{\mathrm{TE},\mathrm{TM}\}$ is the mode's polarization, where TE corresponds to the modes with the electric field lying in the xy plane and TM corresponds to the modes with the magnetic field in the same plane. The imaginary part of electromagnetic Green's functions describes the LDOS and does not diverge due to losses in the system if the emitter is placed in lossless dielectric between the nanorods. On the other hand, material losses in the nanorods themselves and radiation from the resonator into the far field remove divergence of Eq. (1) in the vicinity of the poles.

The rigorous eigenmode analysis of the anisotropic and lossy rectangular resonator requires sophisticated numerical techniques. However, approximate expressions for the eigenfrequencies and field distributions in the resonator can be derived within an approximate analytical formalism [38]. Within this formalism, perfect electric conductor (PEC) boundary conditions are imposed at the sidewalls of the resonator at $x = \pm L_x/2$, $y = \pm L_y/2$ in order to obtain the resonator mode numbers, corresponding to quantized $k_{x,(m)}$ and $k_{y,(l)}$ wave vectors in x and y directions, respectively:

$$\begin{aligned} k_{x,(m)} &= \frac{\pi m}{L_x}, \quad m = 1,3,5\ldots, \\ k_{y,(l)} &= \frac{\pi l}{L_y}, \quad l = 1,3,5\ldots. \end{aligned} \quad (2)$$

If the radiating dipole is situated on the $(0,0,z)$ axis, only the modes with symmetric E_x and E_y field distributions with respect to inversions $x \to -x, y \to -y$ can be excited by the dipole and will contribute to the Purcell effect.

In order to obtain the mode structure in the remaining z direction, a slab waveguide is then considered which may support TM and TE guided modes confined in the z direction. The propagation constant of these modes $k_{\perp,(m,l)}$ satisfies the condition

$$k_{\perp,(m,l)} = \sqrt{k_{x,(m)}^2 + k_{y,(l)}^2}. \quad (3)$$

This $k_{\perp,(m,l)}$ propagation constant can be evaluated by finding the modes of a hyperbolic-metamaterial-slab waveguide in the effective medium approximation [39]. As has been shown in the analysis of the metamaterial waveguides [39] and can also be seen from the numerical modeling below, this approximation holds for lower-order highly confined modes of sufficiently large resonators.

First, we will consider quasi-TE modes of the resonator. By substituting Eq. (2) into the dispersion equation (3) for a slab waveguide which is symmetric with the respect to the $z \to -z$ inversion, we find two classes of modes with the tangential electric field either symmetric ($n = 0, 2, 4, \ldots$) or antisymmetric ($n = 1, 3, 5\ldots$) along the z axis (the index here corresponds to the number of zero crossings for a leading field component: electric field for TE and magnetic field for TM modes):

$$\frac{(k_{\perp,(m,l)}^2 - \left(\frac{\omega_{m,l,n,\mathrm{TE}}}{c}\right)^2)^{1/2}}{(\varepsilon_{xx}\left(\frac{\omega_{m,l,n,\mathrm{TE}}}{c}\right)^2 - k_{\perp,(m,l)}^2)^{1/2}} = \tan\left\{\frac{(\varepsilon_{xx}\left(\frac{\omega_{m,l,n,\mathrm{TE}}}{c}\right)^2 - k_{\perp,(m,l)}^2)^{1/2}L_z}{2} + \frac{\pi}{4}[1-(-1)^n]\right\}. \quad (4)$$

If the dipole is placed at $z = 0$, the antisymmetric modes will have the node of the electric field at the dipole position and thus cannot be excited and will not contribute to the Purcell effect [Eq. (1)]. When the dipole is shifted from $z = 0$, both symmetric and antisymmetric modes will contribute to the Purcell factor. Similarly, using the waveguide dispersion for TM polarized modes, we obtain

$$\frac{(\varepsilon_{xx})^{1/2}\left(k_{x,(m)}^2 + k_{y,(l)}^2 - \left(\frac{\omega_{m,l,n,\mathrm{TM}}}{c}\right)^2\right)^{1/2}}{\left(\left(\frac{\omega_{m,l,n,\mathrm{TM}}}{c}\right)^2 - \frac{k_{\perp,(m,l)}^2}{\varepsilon_{zz}}\right)^{1/2}} = \tan\left\{\frac{(\varepsilon_{xx})^{1/2}(\left(\frac{\omega_{m,l,n,\mathrm{TM}}}{c}\right)^2 - \frac{k_{\perp,(m,l)}^2}{\varepsilon_{zz}})^{1/2}L_z}{2} + \frac{\pi}{4}[1-(-1)^n]\right\}, \quad (5)$$

In this case, however, the modes are symmetric ($n = 0, 2, 4, \ldots$) or antisymmetric ($n = 1, 3, 5\ldots$) with respect to the tangential component of the magnetic field, with the electric field having opposite symmetry.

In order to distinguish the mode contributions to the Purcell effect, the spectrum of the eigenmodes will first be analyzed assuming vanishing Ohmic losses in the metamaterial. In this approximation, following Eq. (4), the TE mode eigenfrequencies are limited by

$$\frac{\pi}{L_x}\sqrt{(m)^2+(l)^2} < \frac{\omega_{m,l,n,\mathrm{TE}}}{c} < \frac{\pi}{L_x}\sqrt{\varepsilon_{xx}}\sqrt{(m)^2+(l)^2}, \quad (6)$$

satisfying the requirement that the left-hand side of Eqs. (2) and (4) should be real valued. Therefore, for any finite-frequency range, only a finite number of pairs (m,l) exists that satisfy Eq. (6). For each (m,l) pair, a finite set of mode numbers n can be found. Thus, in a finite-frequency range, only a finite number of eigenmodes (m,l,n) of the metamaterial resonator exists.

Specifically, for the metamaterial resonator of the square cross section with $L_x = L_y = 900$ nm and $L_z = 350$ nm and the effective permittivity as in Fig. 1(c), the following eigenmodes can be excited in the spectral range from 500 to 1500 nm: TE_{110} at $\lambda = 1450$ nm, TE_{130} and TE_{310} at

$\lambda = 780$ nm, and TE_{330} at $\lambda = 570$ nm. It should be noted that while the predicted higher-order modes were observed in the rigorous numerical simulations of the nanorod composite, the fundamental mode TE_{110} occurs at wavelengths larger than 1500 nm. This is a known discrepancy [40] related to the fact that the simplified analysis used above works worse for the fundamental modes with lower confinement within a resonator, and, thus, the actual frequency of the TE_{110} mode can deviate substantially from the value predicted by the simplified analytical formalism.

Contrary to TE modes, the eigenfrequencies of TM modes decrease with the increase of m and l, as can be seen from Eq. (5). This property of the hyperbolic resonators has been observed both theoretically and experimentally [19] and can be understood from the requirement for the TM eigenfrequencies analogous to Eq. (6):

$$\frac{\pi^2}{L_x^2}[m^2 + l^2] > \frac{\omega_{m,l,n,\mathrm{TM}}^2}{c^2} > \frac{\pi^2}{L_x^2 \varepsilon_{zz}}[(m)^2 + l^2]. \qquad (7)$$

Since ε_{zz} is negative in the hyperbolic regime, the right-hand-side inequality holds for any frequency and m, l. Thus, there exist modes with arbitrary large m, l that satisfy the left-hand-side inequality. The number of the supported modes is, however, limited due to the metamaterial realization as a periodic nanorod array. Contrary to the case of the uniform hyperbolic metamaterial, the x and y wave vectors should be within the first Brillouin zone of the array, $k_{x,y} < \pi/a$, where a is the period of the array. Thus, for TM modes, m and l eigenvalues can be 1, 3, 5, and 7 in the case of the 16×16 nanorod array with the parameters as in Fig. 1. For simplicity, in these analytical calculations, we do not consider possible coupling between TE and TM modes due to three-dimensional geometrical confinement (the numerical modeling includes all such effects).

For each value of m and l there is a number of eigenmodes corresponding to different n. This number is finite and increases with m, l. Despite the large number of the TM polarized eigenmodes supported by the resonator, many of them have a minor contribution to the overall Purcell factor since they have either small Q factors due to the large damping inside the resonator when the losses in metal are considered or a small value of the x component of the electric field at the dipole's position due to the different symmetry properties of the eigenmodes (Fig. 2). Namely, some of the eigenmodes

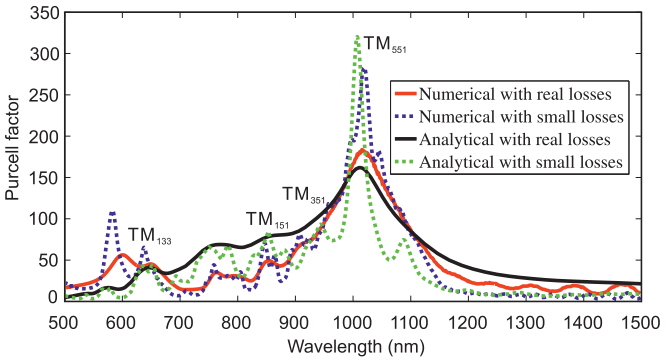

FIG. 2. (Color online) Comparison of the numerical (red and blue lines) and analytical (green and black lines) of the Purcell factor in the case of real losses (solid lines) and reduced losses $\mathrm{Im}(\varepsilon)/10$ (dashed lines). The metamaterial parameters are as in Fig. 1. The resonator size is 16×16 nanorods with $L_x = L_y = 900$ nm. In the numerical simulations we have used a small dipole source placed in the centre of the resonator and oriented along x direction.

would have a minimum of the x component of the electric field at the dipole position, and some would have maxima [41]. Moreover, in the vicinity of the ENZ frequency, the modes with large values of n are excited. These modes, however, have large losses and thus provide little contribution to the overall Purcell effect. It should be noted, however, that calculations of the Purcell enhancement for emitters placed in contact with lossy media face several challenges as the Green's functions diverge [30]. This problem is usually addressed by introducing a depolarization volume (a small lossless cavity) around the emitter [30]. The numerical modeling below does not, however, face the above issues, as the emitter is placed in the lossless space between the actual rods, forming the metamaterial.

The dependences of the resonant wavelength on the resonator height L_z for modes TE_{130}, TM_{151}, and TM_{551} are shown in Fig. 3(a). The higher-order mode TM_{551} is lower in frequency than the lower-order mode TM_{151}, as is expected for the hyperbolic resonators. This can be intuitively understood considering PEC boundary conditions on the interface perpendicular to the z axis. In this case, k_z is simplified to $k_z = \pi n L_z = (\varepsilon_{xx})^{1/2}(\omega^2/c^2 - k_\perp^2/\varepsilon_{zz})^{1/2}$, where n is an integer. It can be seen that for fixed n, the eigenfrequency

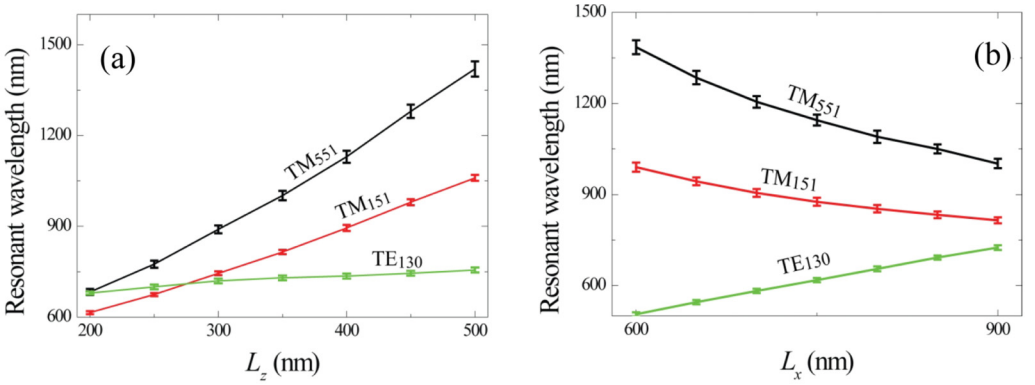

FIG. 3. (Color online) Dependence of the eigenmode wavelengths on (a) L_z for the fixed $L_x = L_y = 900$ nm and (b) L_x for fixed $L_z = 350$ nm. Bars indicate the width of the resonance.

decreases with increasing $k_\perp$. The dependence of the resonant wavelength on the resonator width L_x at the fixed resonator length $L_z = 350$ nm is shown in Fig. 3(b). As we can see, the resonant wavelengths of the TM modes decrease with the increase of the resonator lateral size. This behavior is evident from Eq. (3) since it can be seen that for the fixed value of k_z^{TM} the resonant frequency should increase with increasing L_x. In contrast, the wavelengths of the TE modes increase with the increase of the resonator width L_x, similar to the case of a conventional anisotropic dielectric resonator.

B. Purcell enhancement due to the hyperbolic resonator modes

The analytical analysis performed above does not account for either the microscopic structure of the metamaterial or the radiation from the resonator. We now compare the effective medium analytical description to the results of the numerical modeling in the case of an x-polarized dipole placed in the center of the 16×16 array of Au nanorods (period $a = 60$ nm and radius $r = 15$ nm) which corresponds to the resonator dimensions $L_y = L_x = 900$ nm and $L_z = 350$ nm. We have considered real losses in gold for comparison to the analytical model as well as artificial low losses (artificially reduced by 10 times) in order to articulate the mode position (Fig. 2). The analytical model provides a clear correspondence to the numerical results, and the individual eigenmodes can be identified. The highest Purcell factor corresponds to the excitation of the TM_{551} eigenmode in the vicinity of 1000 nm. The Purcell factor near the ENZ frequency range does not have extremely large values, as would be expected in the case of an infinitely large metamaterial [30].

C. Saturation of the Purcell enhancement in finite-size arrays

The Purcell factor for the electric dipole placed in the center of the metamaterial resonator was numerically calculated for different sizes of the resonator (Fig. 4). Both parallel and perpendicular to the nanorods, orientations of the emitting dipole were analyzed in square and rectangular resonators with up to 18 rods in one direction. The obtained dependence of the Purcell factor shows a fast convergence with an increasing number of rods in the array. In fact, in the arrays larger than 16×16 rods (900×900 nm), the Purcell factor approaches the values for the infinite (in the x and y directions) planar metamaterial slab, so that the Purcell factors for 16×16 and 18×18 arrays are essentially the same without the signatures of the resonant modes of the resonator due to the reduced quality factor of the modes [Fig. 4(a)]. This quality factor reduction in larger systems is the result of increased material losses due to the mode being spread over larger number of rods. Rectangular nanorod arrays show similarly fast convergence, leading to the conclusion that the behavior of 16×16 nanorod structures is extremely close to that of the infinite metamaterial [Fig. 4(a)].

The x-oriented dipole source which is located in the central part of the array can excite only even modes [Fig. 4(a)]. It can be seen that for the 2×2 array the highest Purcell factor (around 500) is reached at 950-nm wavelength (due to the small number of the rods forming the resonator, the identification of the mode structure of the resonator is not possible in the effective medium formalism as in Sec. III A). The highest Purcell factor obtained for the smallest array can be attributed to a small modal volume. For larger arrays this mode exhibits a slight shift to longer wavelengths, as expected from Eq. (4), and the Purcell factor decreases up to the value of 200. The Purcell factor for a z-oriented dipole is very low but also follows the mode structure of the resonator with the increasing number of rods [Fig. 4(b)]. The rectangular nanorod arrays provide a Purcell factor of around 200 already for two rows of nanorods [Fig. 4(c)]. The contribution of different transverse modes of the rectangular array in the Purcell factor is more pronounced for arrays with a smaller number of rows and becomes indistinguishable for arrays with six or more rows of rods [Fig. 4(c), green curve]. For all considered sizes of the resonators, a Purcell factor of less than 100 is observed in the ENZ regime at around 520-nm wavelength [Fig. 1(c)]. As one can see from the consideration of rectangular metamaterial resonators, the optical response of the finite-size resonators converges quickly to the response of the infinitely extended metamaterial slabs.

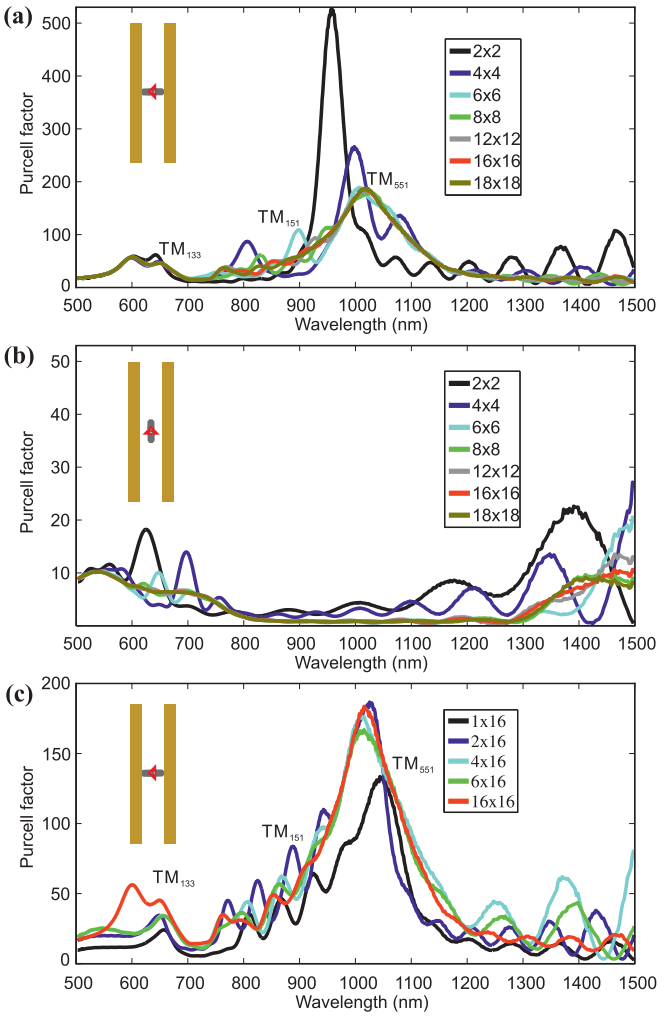

FIG. 4. (Color online) The Purcell factor dependence on the number of nanorods in (a) and (b) square and (c) rectangular resonators for an emitting dipole (a) and (c) perpendicular and (b) parallel to the nanorods. The dipole is located in the center of the array.

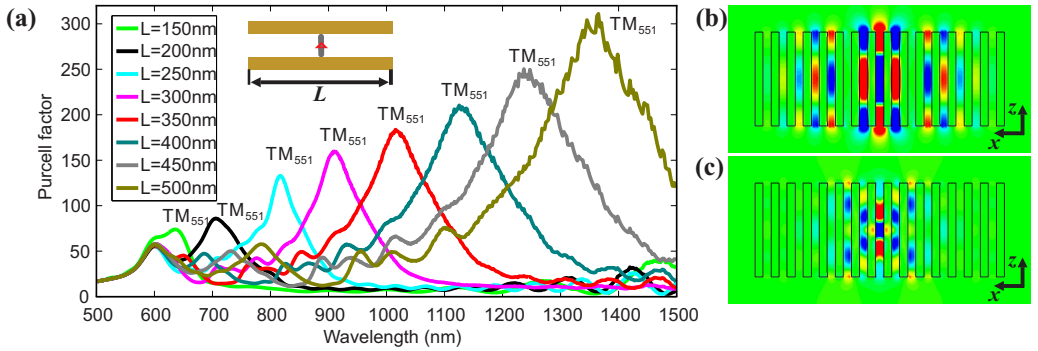

FIG. 5. (Color online) (a) The Purcell factor dependence on the height of the hyperbolic metamaterial resonator (16 × 16 nanorod array, $L_x = L_y = 900$ nm). (b), (c) The electric field E_x distributions excited by the dipole positioned at the center of the resonator with $L_z = 350$ nm at the wavelength of (b) 1000 nm and (c) 600 nm (nonresonant wavelength).

D. Purcell enhancement dependence on the rod length

We will now investigate the impact of the resonator height (rod length) on the Purcell factor (Fig. 5). In this section, resonators made of an array of 16 × 16 rods were considered. For all nanorod heights, there is a relatively small peak in the vicinity of the ENZ frequency related to the high modal density of bulk plasmon-polariton modes at this frequency [39,42]. The highest observed Purcell factor strongly depends on the rod length. Its maximum shifts to longer wavelengths with the increase in rod height, in accordance with the frequency shift of the resonator mode [Eq. (4)]. This (TM_{551}) mode has a characteristic field distribution inside the resonator [Fig. 5(b)] with three pronounced maxima of the electric field (two maxima of the magnetic field with one zero crossing), typical of the second Fabry-Pérot TM mode along the rods. Away from the modes of the resonator, the electric field has the characteristic cross-shaped form [Fig. 5(c)] typical for a radiating dipole field distribution in a hyperbolic dispersion regime [12].

E. Purcell enhancement in small hyperbolic resonators

If, starting from a single nanorod, the number of rods in the resonator is gradually increased, nontrivial behavior of the Purcell factor is observed (Fig. 6). The highest Purcell factor is obtained neither with a single rod nor in the limit of an infinite number of rods. The optimal structure provides a resonant mode with a high LDOS which enhances the decay rate. It can be seen that the dipole positioned near the center of a single nanorod excites the second-order mode $n = 2$ with three maxima of the electric field [Fig. 6(b)] at a wavelength of around 855 nm and the fourth mode $n = 4$ with five field maxima [Fig. 6(c)] at a wavelength of around 610 nm. Adding more nanorods to the resonator and thus changing its size and the modal structure lead to a shift of the resonant frequencies in the red spectral range, in accordance with Eq. (4). In particular, for the geometry with four nanorods, the second mode is excited at a wavelength of ∼940 nm [Fig. 6(d)], and the fourth mode is excited at a wavelength of ∼640 nm [Fig. 6(e)]. As mentioned above, the dipole located near the middle section of the nanorod layer can only couple to even modes.

F. Purcell enhancement dependence on the dipole position.

In order to understand the average Purcell factor for an ensemble of randomly distributed emitters, the position-dependent Purcell factor has been investigated. When the position of the emitter is changed along the nanorod length from just outside the metamaterial towards the center of the metamaterial layer, the Purcell factor has four maxima, which correspond to the four lowest modes of the resonator (Fig. 7). The odd modes were not excited by the dipole situated at the central point of the array due to symmetry-induced

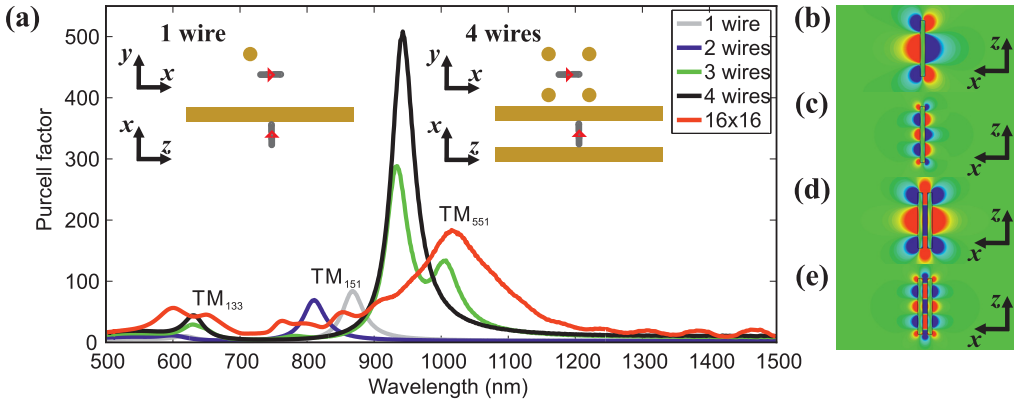

FIG. 6. (Color online) (a) Comparison of the Purcell factor for different numbers of plasmonic rods forming a resonator. (b)–(e) The electric fields E_x of the dipole (b) and (c) near a single nanorod and (d) and (e) near a four-nanorod array at the wavelengths of (b) 856 nm, (c) 611 nm, (d) 937 nm. and (e) 637 nm.

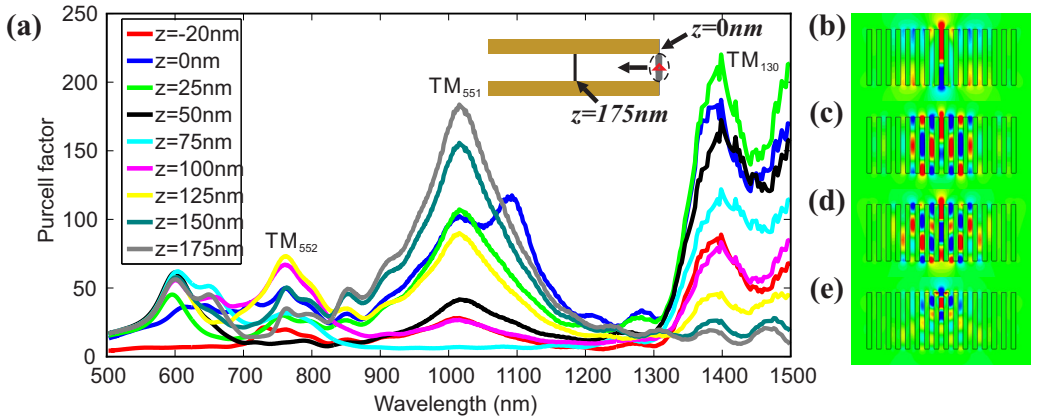

FIG. 7. (Color online) (a) The Purcell factor dependence on an emitter position inside the metamaterial resonator with $L_z = 350$ nm and $L_x = L_y = 900$ nm. The coordinate $z = 0$ corresponds to the edge of the hyperbolic medium. (b)–(e) The electric field E_x distributions excited by the dipole positioned at $z = 0$ for the wavelengths of (b) 1363 nm (TM_{130} mode, first Fabry-Pérot resonance $n = 0$, with two electric field maxima, one magnetic field maximum, no magnetic field zero crossing), (c) 1000 nm (TM_{551} mode, second Fabry-Pérot resonance $n = 1$ with three electric field maxima, two magnetic field maxima, one magnetic field zero crossing), (d) 750 nm (TM_{552} mode, third Fabry-Pérot resonance $n = 2$ with four electric field maxima, three magnetic field maxima, two magnetic field zero crossings), and (e) 600 nm (nonresonant wavelength). All other parameters are as in Fig. 3.

selection rules. It can be seen from the LDOS spectrum [Fig. 7(a)] that the efficiency of the excitation of the resonator modes depends on the local field strength of a particular mode at the position of the radiating dipole. It can be seen that at different dipole positions, preferential excitation of the modes TM_{130} (two electric field maxima, one magnetic field maximum, no magnetic field zero crossing), TM_{551} (three electric field maxima, two magnetic field maxima, one magnetic field zero crossing), and TM_{552} (four electric field maxima, three magnetic field maxima, two magnetic field zero crossings) occurs at the wavelengths of 1363, 1000, and 750 nm, respectively. For the shorter wavelength of 600 nm, the electric field is shaped as an inverted V [Fig. 7(e)], typical of the nonresonant hyperbolic regime. The Purcell factor drops off very quickly with increasing distance between the dipole and the metamaterial surface: dipoles situated more than 20 nm away from the interface do not exhibit any significant Purcell enhancement (Fig. 7).

IV. CONCLUSION

A comprehensive numerical and analytical analysis of the Purcell enhancement in finite-size nanorod metamaterial resonators was performed. Using a nanorod metamaterial with hyperbolic dispersion of electromagnetic modes, the resonators with a complex hierarchy of modes can be realized. We have shown that the modes of the hyperbolic resonator are responsible for the enhancement of spontaneous emission rates of emitters placed inside the resonator. Thus, a controllable Purcell enhancement can be achieved in the desired wavelength range by choosing appropriate resonator sizes. A detailed analysis of various types of geometrical arrangements of the metamaterial and emitter was carried out. The results suggest that finite-size metamaterial resonators with properly designed modes outperform infinite metamaterials in terms of radiation efficiency enhancement. It was shown that the influence of only the 16×16 nanorod array on the dipole emission properties converges to that of an infinite metamaterial. These findings can provide guidelines for modeling and optimization of experimental samples. As for an outlook for possible future applications, it is worth mentioning nanostructured light-emitting devices with high-speed switching rates, cavities for surface plasmon amplification by stimulated emission of radiation (SPASERs), and sensing applications.

ACKNOWLEDGMENTS

The authors would like to thank Prof. Yuri S. Kivshar for useful discussions. This work has been supported, in part, by EPSRC (UK), the ERC iPLASMM project (321268), US Army Research Office (W911NF-12-1-0533) and Australian Research Council. P.S. is grateful for the support from CONACYT. G.A.W. acknowledges support from the EC FP7 project 304179 (Marie Curie Actions). A.V.Z. acknowledges support from the Royal Society and the Wolfson Foundation and rejects any involvement in the grants, listed below. The work of I.I., A.S.S., P.A.B. was supported by the Ministry of Education and Science of the Russian Federation, by the Government of the Russian Federation (Grant 074-U01), by Russian Fund for Basic Research (15-02-01344 and 14-22-02064 ofi-m). I.I. acknowledges Grant of the President of Russian Federation (MK-5220.2015.2). The numerical simulations and investigating of the field distributions has been partially funded by the Russian Science Foundation (Grant No. 14-12-01227). A.P.S. acknowledges Russian Foundation for Basic Research (Project No. 14-02-31783).

[1] L. Novotny and B. Hecht, *Principles of Nano-optics* (Cambridge University Press, Cambridge, 2006).
[2] E. M. Purcell, Phys. Rev. **69**, 681 (1946).
[3] A. Hayat, P. Ginzburg, and M. Orenstein, Phys. Rev. Lett. **103**, 023601 (2009).
[4] A. N. Poddubny, P. Ginzburg, P. A. Belov, A. V. Zayats, and Y. S. Kivshar, Phys. Rev. A **86**, 033826 (2012).
[5] K. J. Vahala, Nature (London) **424**, 839 (2003).
[6] P. Ginzburg, A. V. Krasavin, D. Richards, and A. V. Zayats, Phys. Rev. A **90**, 043836 (2014).
[7] D. K. Gramotnev and S. I. Bozhevolnyi, Nat. Photonics **4**, 83 (2010).
[8] L. Novotny and N. van Hulst, Nat. Photonics **5**, 83 (2011).
[9] J.-J. Greffet, Science **308**, 1561 (2005).
[10] A. V. Akimov, A. Mukherjee, C. L. Yu, D. E. Chang, A. S. Zibrov, P. R. Hemmer, H. Park, and M. D. Lukin, Nature (London) **450**, 402 (2007).
[11] A. G. Curto, G. Volpe, T. H. Taminiau, M. P. Kreuzer, R. Quidant, and N. F. van Hulst, Science **329**, 930 (2010).
[12] P. Shekhar, J. Atkinson, and Z. Jacob, Nano Convergence **1**, 1, (2014).
[13] Z. Jacob, J. Kim, G. V. Naik, A. Boltasseva, E. E. Narimanov, and V. M. Shalaev, Appl. Phys. B **100**, 215 (2010).
[14] A. N. Poddubny, P. A. Belov, P. Ginzburg, A.V. Zayats, and Y. S. Kivshar, Phys. Rev. B **86**, 035148 (2012).
[15] W. Yan, M. Wubs, and N. A. Mortensen, Phys. Rev. B **86**, 205429 (2012).
[16] T. Tumkur, G. Zhu, P. Black, Yu. A. Barnakov, C. E. Bonner, and M. A. Noginov, Appl. Phys. Lett. **99**, 151115 (2011).
[17] H. N. S. Krishnamoorthy, Z. Jacob, E. Narimanov, I. Kretzschmar, and V. M. Menon, Science **336**, 205 (2012).
[18] P. Ginzburg, F. J. Rodríguez Fortuño, G. A. Wurtz, W. Dickson, A. Murphy, F. Morgan, R. J. Pollard, I. Iorsh, A. Atrashchenko, P. A. Belov, Y. S. Kivshar, A. Nevet, G. Ankonina, M. Orenstein, and A. V. Zayats, Opt. Express **21**, 14907 (2013).
[19] X. Yang, J. Yao, J. Rho, X. Yin, and X. Zhang, Nat. Photonics **6**, 450 (2012).
[20] Y. He, S. He, and X. Yang, Opt. Lett. **37**, 2907 (2012).
[21] A. Leviyev, B. Stein, T. Galfsky, H. Krishnamoorthy, I. L. Kuskovsky, V. Menon, and A. B. Khanikaev, arXiv:1505.05438.
[22] Z. Sun, Á. Gutiérrez-Rubio, D. N. Basov, and M. M. Fogler, Nano Lett. **15**, 4455 (2015).
[23] B. M. Wells, A. V. Zayats, and V. A. Podolskiy, Phys. Rev. B **89**, 035111 (2014).
[24] J. Elser, R. Wangberg, V. A. Podolskiy, and E. Narimanov, Appl. Phys. Lett. **89**, 261102 (2006).
[25] M. Silveirinha and N. Engheta, Phys. Rev. Lett. **97**, 157403 (2006).
[26] A. Alù, M. G. Silveirinha, A. Salandrino, and N. Engheta, Phys. Rev. B **75**, 155410 (2007).
[27] E. Forati and G. W. Hanson, New J. Phys. **15**, 123027 (2013).
[28] P. Ginzburg and A. V. Zayats, ACS Nano **7**, 4334 (2013).
[29] N. A. Mortensen, S. Raza, M. Wubs, T. Søndergaard, and S. I. Bozhevolnyi, Nat. Commun. **5**, 3809 (2014).
[30] V. A. Podolskiy, P. Ginzburg, B. Wells, and A. V. Zayats, Faraday Discuss. **178**, 61 (2015).
[31] CST MICROWAVE STUDIO 2014, http://www.cst.com.
[32] P. B. Johnson and R. W. Christy, Phys. Rev. B **6**, 4370 (1972).
[33] A. P. Slobozhanyuk, A. N. Poddubny, A. E. Krasnok, and P. A. Belov, Appl. Phys. Lett. **104**, 161105 (2014).
[34] A. E. Krasnok, A. P. Slobozhanyuk, C. R. Simovski, S. A. Tretyakov, A. N. Poddubny, A. E. Miroshnichenko, Y. S. Kivshar, and P. A. Belov, Sci. Rep. **5**, 12956 (2015).
[35] M. Agioand and A. Alu, *Optical Antennas* (Cambridge University Press, Cambridge, 2013).
[36] W. Vogel and D.-G. Welsch, *Quantum Optics*, 3rd rev. ed. (Wiley-VCH, Berlin, 2006).
[37] F. Intravaia and K. Busch, Phys. Rev. A **91**, 053836 (2015).
[38] A. K. Okaya and L. F. Barash, Proc. IRE **50**, 2081 (1962).
[39] N. Vasilantonakis, M. E. Nasir, W. Dickson, G. A. Wurtz, and A. V. Zayats, Laser Phot. Rev. **9**, 345 (2015).
[40] R. K. Moniga and A. Ittipiboon, IEEE Trans. Antennas Propag. **45**, 1348 (1997).
[41] F. Lemoult, M. Fink, and G. Lerosey, Nat. Commun. **3**, 889 (2012).
[42] S. V. Zhukovsky, O. Kidwai, and J. E. Sipe, Opt. Express **21**, 14982 (2013).